Supporting information

Three-dimensional Carbon Foam-Metal Oxides based Asymmetric Electrodes for High-performance Solid-state Micro-Supercapacitor

Sumana Kumar[1] and Abha Misra[1*]

[1]Department of Instrumentation and Applied Physics, Indian Institute of Science, Bangalore, Karnataka 560012

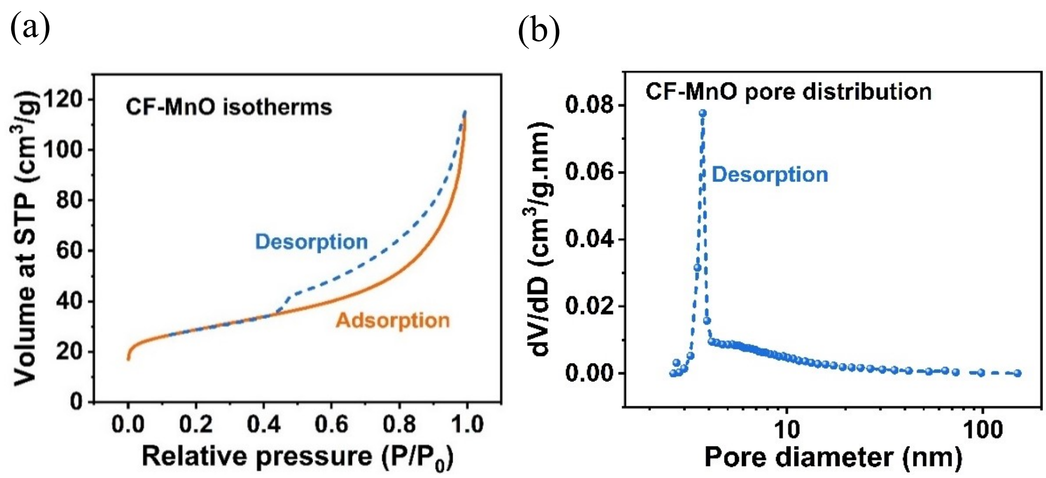

Figure S1: (a) Nitrogen adsorption-desorption isotherms for CF-MnO composite. (b) pore size distribution of CF-MnO composite.

Table S1: Calculated total specific surface area S_{BET}, total pore volume V_T, total micropore volume V_M, micropore surface area S_M, external surface area S_E, average pore diameter d_M for CF, and CF-MnO listed below.

	S_{BET} $m^2\ g^{-1}$	**V_T $cm^3\ g^{-1}$**	**V_M $cm^3\ g^{-1}$**	**S_M $m^2\ g^{-1}$**	**S_E $m^2\ g^{-1}$**	**d_M nm**
CF	209.3	0.2916	0.03	63.39	145.91	5.574
CF-MnO	98.22	0.1781	0.0172	35.9	62.32	9.224

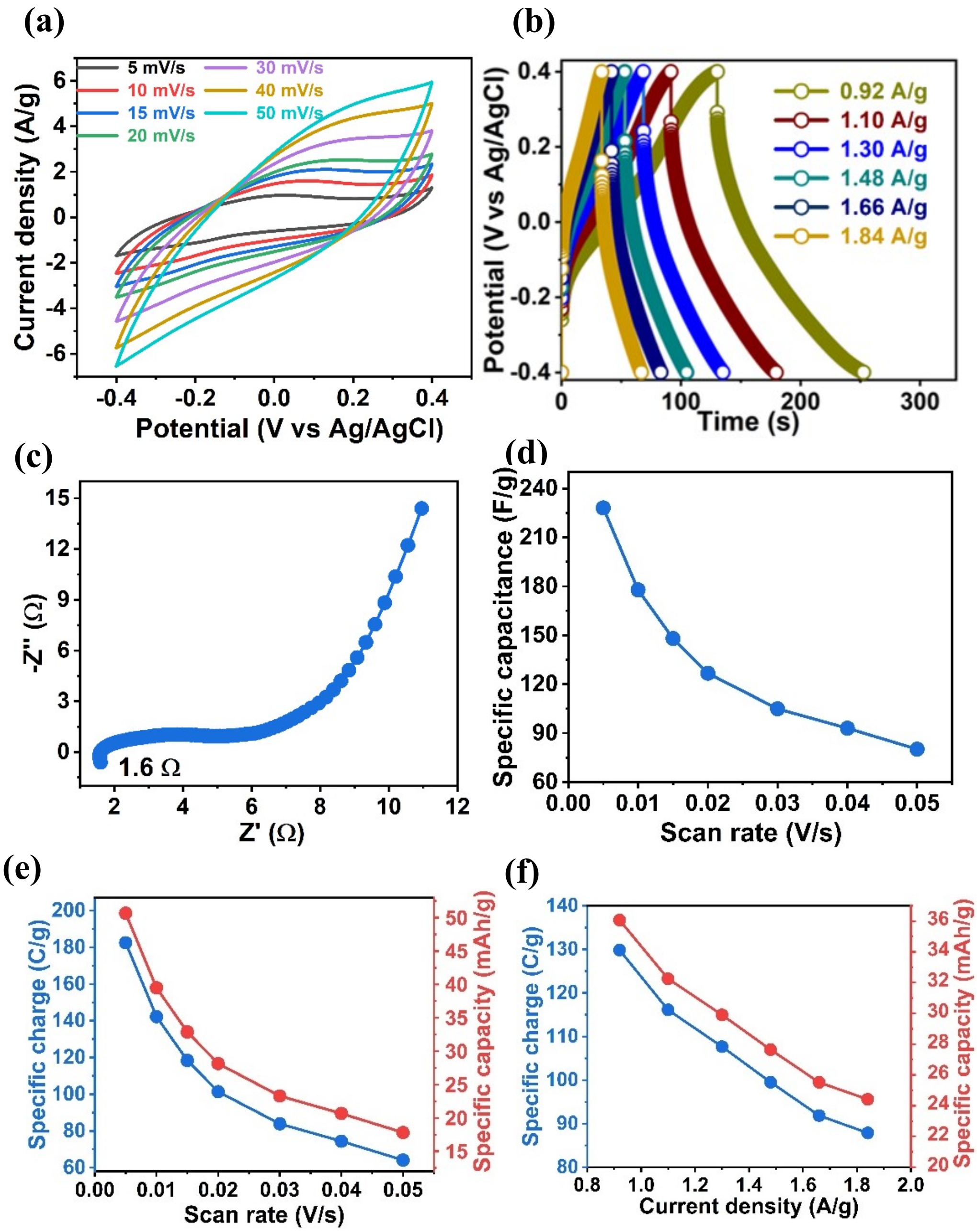

Figure S2: Electrochemical performance of positive electrode material in 6M KOH electrolyte. (a) *CV* curves of CF-MnO (3:1) electrode measured at different scan rates. (b) Galvanostatic charge-discharge curve of CF-MnO (3:1) electrode at various current densities. (c) Nyquist plot of CF-MnO (3:1) electrode. (d) The specific capacitance of CF-MnO (3:1) calculated from *CV* curves as a function of scan rates. (e) The specific charge and capacity of CF-MnO (3:1) calculated from *CV* curves as a function of scan rates. (f) The specific charge and capacity of CF-MnO (3:1) calculated from *CD* curves as a function of current densities.

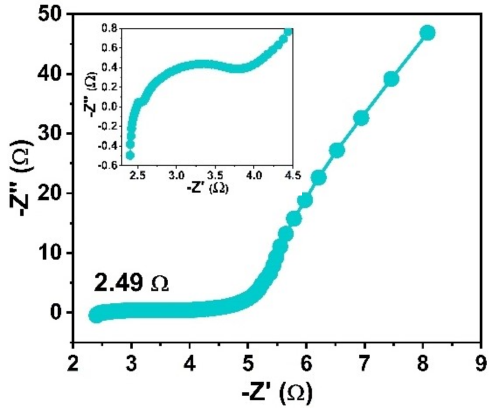

Figure S3: Nyquist plot of pristine CF electrode. Inset shows a magnified view in the high-frequency region.

.

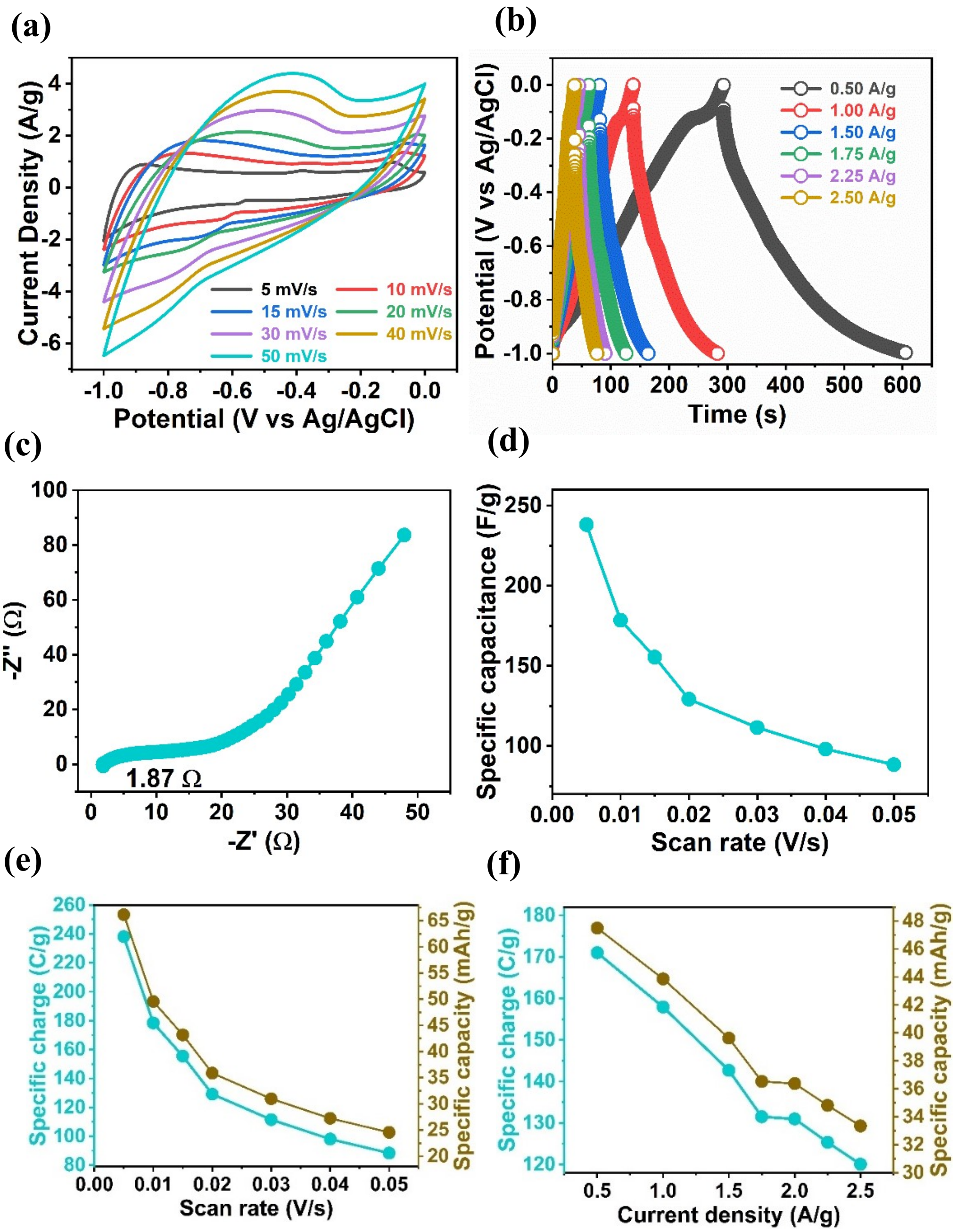

Figure S4: The electrochemical performance of negative electrode material in 6 M KOH electrolyte. a) CV curves of CF-Fe_2O_3 (9:1) at various scan rates ranging from 5 to 50 mV/s. b) Galvanostatic charge-discharge curves of CF-Fe_2O_3 (9:1) at different current densities. c) Nyquist plot of CF-Fe_2O_3 (9:1) in the frequency ranging from 0.01 Hz to 1k Hz. d) Specific capacitance of CF-Fe_2O_3 (9:1) calculated from *CV* curves as a function of scan rates. e) The specific charge and capacity of CF-Fe_2O_3 (9:1) calculated from *CV* curves as a function of scan rates. (f) The specific charge and capacity of CF-Fe_2O_3 (9:1) calculated from *CD* curves as a function of current densities.

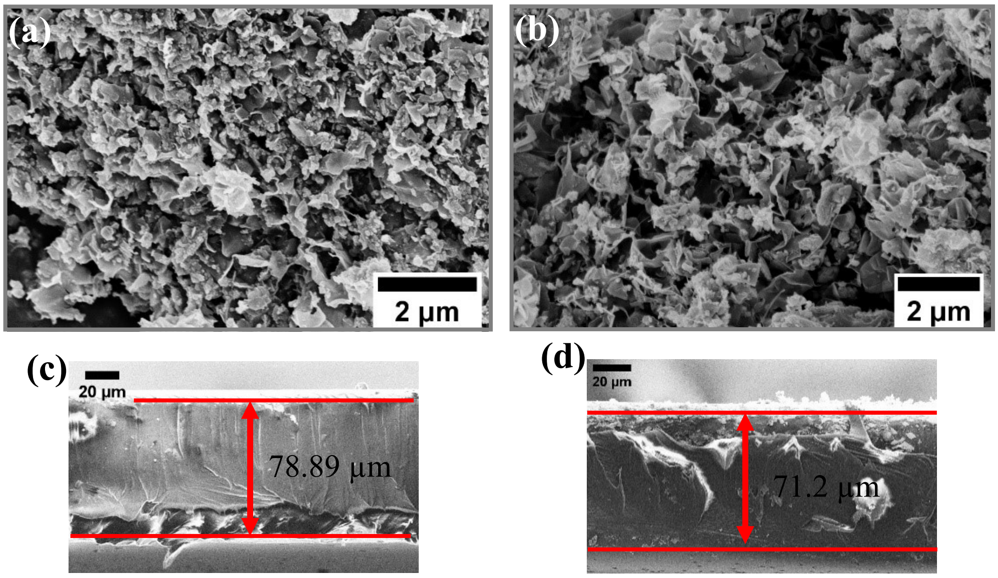

Figure S5: Morphological and structural characterization of spray printed asymmetric micro-supercapacitor. Top-view SEM image of (a) CF-Fe_2O_3 coated negative microelectrodes, (b) CF-MnO coated positive microelectrodes. Cross-sectional SEM image of (c) CF-Fe_2O_3 composite coated negative electrode, (d) CF-MnO composite coated positive electrode.

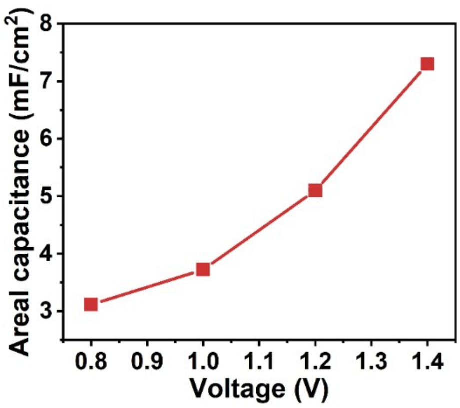

Figure S6: Areal capacitance of CF-MnO//CF-Fe_2O_3 device calculated from the *CV* curves with varying voltage window from 0.8 to 1.4 V.

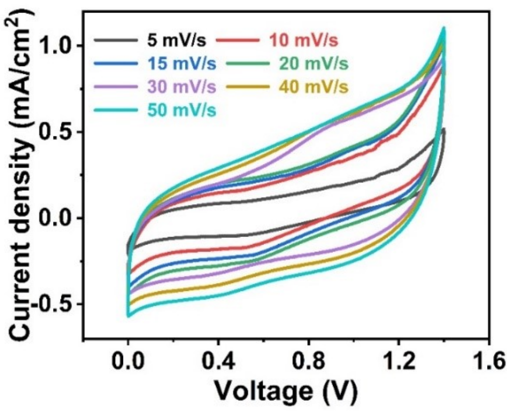

Figure S7: *CV* curves of asymmetric CF-MnO//CF-Fe_2O_3 micro-supercapacitor at scan rates ranging from 5 to 50 mV/s.

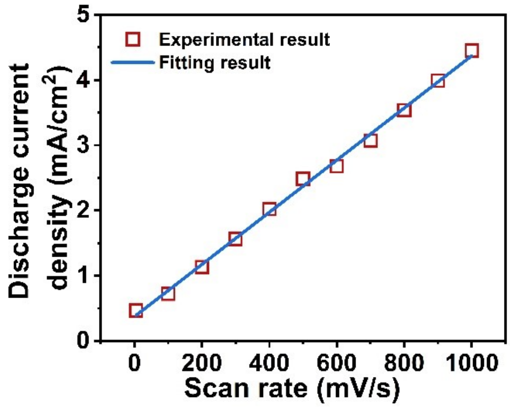

Figure S8: The discharge current density plotted with each corresponding scan rate of the CF-MnO//CF-Fe_2O_3 device.

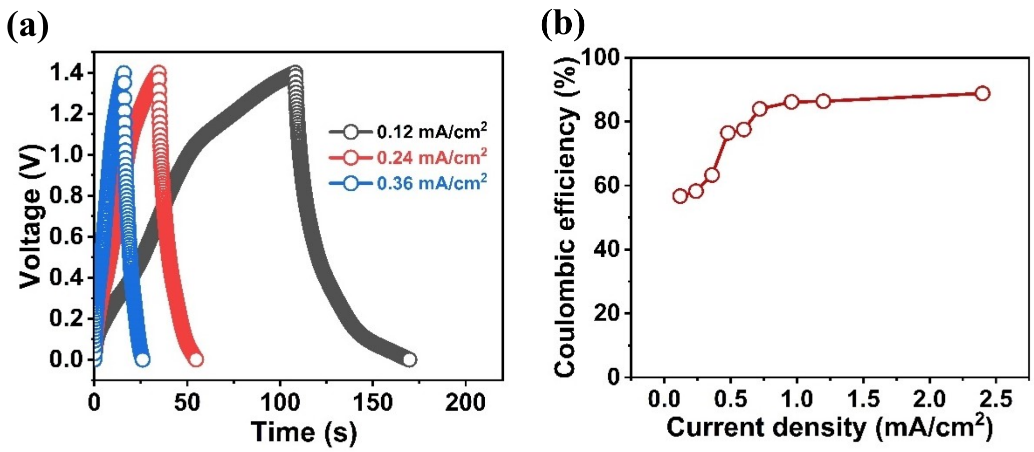

Figure S9: (a) Galvanometric charge-discharge curve for asymmetric micro-supercapacitor with various current densities. (b) Coulombic efficiency plotted against applied current densities.

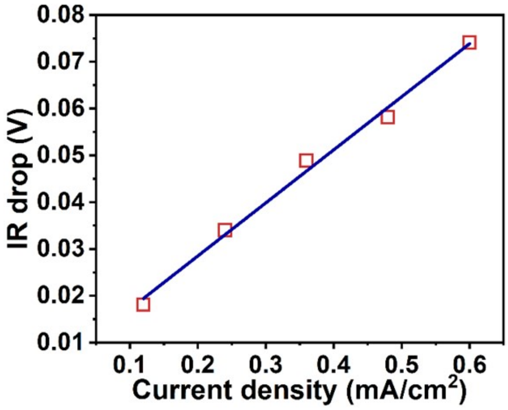

Figure S10: The voltage drop or IR drop plotted with each corresponding applied current density of the CF-MnO//CF-Fe_2O_3 device.

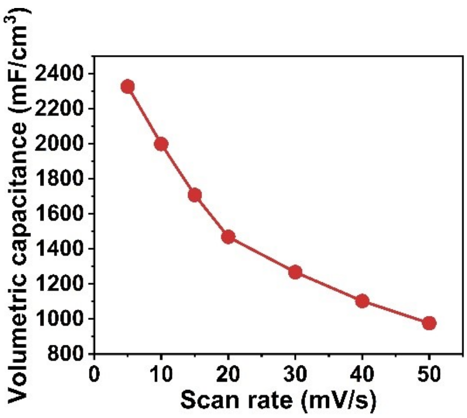

Figure S11: Volumetric capacitance of CF-MnO//CF-Fe_2O_3 asymmetric micro-supercapacitor versus scan rate.

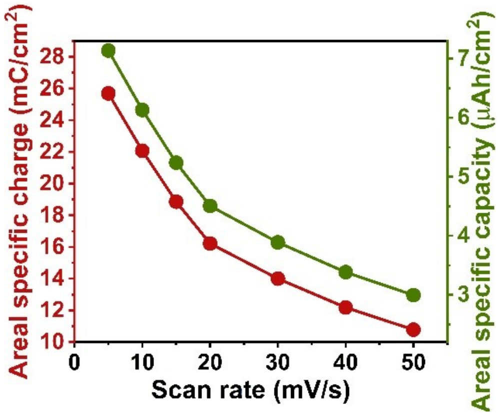

Figure S12: Areal specific charge and areal specific capacity versus scan rate of the asymmetric micro-supercapacitor.

Table S2: The areal specific capacitance versus applied current density of the asymmetric micro-supercapacitor.

Current density (mA/cm^2)	Areal specific capacitance (mF/cm^2) $C_A = \frac{2I\int V dt}{A \times V^2 \vert_{V_i}^{V_f}}$
0.12	2.24
0.24	1.86
0.36	1.62
0.48	1.51
0.60	1.43
0.72	1.41
0.96	1.34
1.2	1.35

Table S3: Comparison of equivalent series resistance (R_s) with reported interdigitated asymmetric micro-supercapacitor.

Asymmetric micro-supercapacitor structure	Equivalent series resistance (R_s)	Ref
VN//MnO_2	70 Ω	[1]
MnO_2/MWNT//VWMWNT	42 Ω	[2]
NiCoP@NiOOH//ZIF-C	21.3 Ω	[3]
PNG//PNG-MoO_2	55 Ω	[4]
MXene//AC	15 Ω	[5]
CF-MnO//CF-Fe_2O_3	13.5 Ω	This work

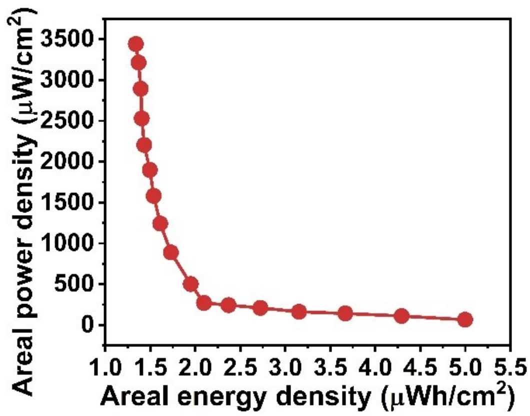

Figure S13: Ragone plot of the asymmetric micro-supercapacitor calculated from CV curves.

Table S4: The voltage excluding IR drop (V-IR) with each corresponding current density of the asymmetric micro-supercapacitor.

Current density mA/cm^2	**V-IR** V
0.12	1.382
0.24	1.367
0.36	1.351
0.48	1.342
0.60	1.326
0.72	1.325
0.96	1.333
1.2	1.314
2.4	1.269
3.6	1.273

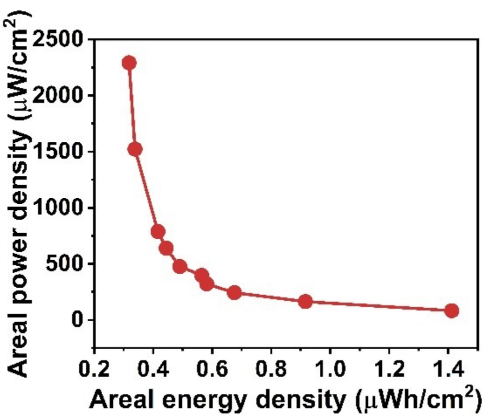

Figure S14: Ragone plot of the asymmetric micro-supercapacitor calculated from *CD* curves.

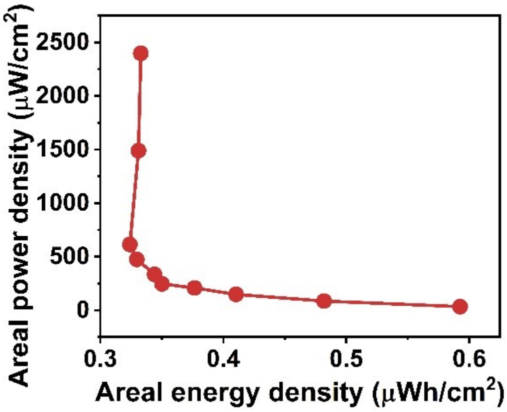

Figure S15: Ragone plot of the asymmetric micro-supercapacitor calculated from *CD* curves using integral formula.

Table S5: Comparison of capacitance retention with reported interdigitated asymmetric micro-supercapacitor.

Asymmetric micro-supercapacitor structure	Electrolyte	Retention (cycles)	Ref
$Ti_3C_2T_x$//MnO_2/PPy	PVA/H_2SO_4	80.7% (5000)	[6]
MnO_2// Fe_2O_3	1 M KOH	80% (2,500)	[7]
Ti_3C_2//MnO_2	PVA/LiCl	87% (10000)	[8]
MXene//AC	PVA/Na_2SO_4	91.4% (10000)	[5]
PNG//PNG-MoO_2	PVA/LiCl	88% (10000)	[4]
rGO//rGO/Mn_3O_4	PVA/LiCl	94% (3000)	[9]
VO_x/rGO//G-VNQDs/rGO	PVA/LiCl	65% (8000)	[10]
MnO_2/MWNT//VWMWNT	PMMA-PC-$LiClO_4$	86% (10000)	[2]
NiCoP@NiOOH//ZIF-C	PVA/KOH	86% (8000)	[3]
VN//MnO_2	“Water-in-salt” gel SiO_2-LiTFSI	90% (5000)	[1]
CF-MnO//CF-Fe_2O_3	PVA-KOH	86% (10000)	This

			work

References:

1 J. Qin, S. Wang, F. Zhou, P. Das, S. Zheng, C. Sun, X. Bao and Z. S. Wu, *Energy Storage Mater.*, 2019, **18**, 397–404.

2 J. Yun, Y. Lim, H. Lee, G. Lee, H. Park, S. Y. Hong, S. W. Jin, Y. H. Lee, S. S. Lee and J. S. Ha, *Adv. Funct. Mater.*, 2017, **27**, 1–13.

3 M. Qiu, P. Sun, G. Cui, Y. Tong and W. Mai, *ACS Nano*, 2019, **13**, 8246–8255.

4 L. Zhang, Z. Chen, S. Zheng, S. Qin, J. Wang, C. Chen, D. Liu, L. Wang, G. Yang, Y. Su, Z. S. Wu, X. Bao, J. Razal and W. Lei, *J. Mater. Chem. A*, 2019, **7**, 14328–14336.

5 Y. Xie, H. Zhang, H. Huang, Z. Wang, Z. Xu, H. Zhao, Y. Wang, N. Chen and W. Yang, *Nano Energy*, 2020, **74**, 104928.

6 X. Li, Y. Ma, P. Shen, C. Zhang, M. Cao, S. Xiao, J. Yan, S. Luo and Y. Gao, *Adv. Mater. Technol.*, 2020, **5**, 1–8.

7 Z. Liu, X. Tian, X. Xu, L. He, M. Yan, C. Han, Y. Li, W. Yang and L. Mai, *Nano Res.*, 2017, **10**, 2471–2481.

8 F. Zhao, W. Liu, T. Qiu, W. Bin Gong, W. Ma, Q. Li, F. Li and F. Geng, *ACS Nano*, 2020, **14**, 603–610.

9 X. Wang, F. Wan, L. Zhang, Z. Zhao, Z. Niu and J. Chen, *Adv. Funct. Mater.*, 2018, **28**, 1–9.

10 K. Shen, J. Ding and S. Yang, *Adv. Energy Mater.*, 2018, **8**, 1–7.